16th Australasian Fluid Mechanics Conference
Crown Plaza, Gold Coast, Australia
2-7 December 2007

Spatio-temporal stability analysis of the separated flow past a NACA 0015 airfoil with ZNMF jet control

V. Kitsios[1], A. Ooi[1] and J. Soria[2]

[1]Walter Bassett Aerodynamics Laboratory
University of Melbourne, Victoria, 3010 AUSTRALIA

[2]Laboratory For Turbulence Research in Aerospace and Combustion
Monash University, 3800 AUSTRALIA

Abstract

The current paper presents the spatio-temporal stability analysis of an instance of laminar separation, with the intention of determining the most appropriate forcing frequency to initiate flow reattachment. The flow configuration is a NACA 0015 airfoil at an angle of attack (α) where laminar separation occurs immediately downstream of the leading edge. A zero-net-mass-flux (ZNMF) jet, normal to the surface and spanning the entire leading edge is used to achieve reattachment. The uncontrolled flow field was generated numerically in [5] using a three-dimensional (3-D) Large Eddy Simulation (LES) and compared to the complementary water tunnel experiments of [22]. Initial simulations of the uncontrolled case agree well with the PIV and force measurements. The stability analysis presented herein is undertaken on the mean velocity field of the LES. The frequency determined by the stability analysis to maximise spatial growth of the disturbance is finally compared to the forcing frequency that maximised lift enhancement in the experimental study.

Introduction

The control of separation in a laminar separated boundary layer is inherently linked to the initiation of the transition to turbulence. Laminar separation occurs due to the presence of an adverse pressure gradient (APG). In the present case, the APG is applied via the curvature of the airfoil surface with respect to the freestream. Laminar velocity profiles on the verge of separation are significantly more unstable to small disturbances as opposed to those with a healthy velocity profile [14]. The former are therefore more amenable to transition to turbulence for a given disturbance level in the environment, or an actively applied control. If the flow becomes turbulent, by virtue of the enhanced mixing, higher momentum fluid is drawn toward the wall and the potential for reattachment is increased. The problem of determining the frequency that best promotes reattachment in a laminar separated boundary layer, is therefore, equivalent to determining the frequency that best initiates transition to turbulence. The latter can be determined using the perturbation form of the *Navier Stokes Equations* (NSE) to determine the frequency that will maximise the spatial growth of a disturbance.

Proper selection of the forcing frequency ensures that a lower control amplitude is required and hence less energy expended to achieve the desired goal. This was illustrated in the study of [16], when both steady and oscillatory tangential blowing was applied to achieve a lift enhancement on a NACA 0015 airfoil for a Reynolds number based on chord length of $Re_c = 1 \times 10^6$. This study found that an order of magnitude less energy was required for an oscillatory jet to achieve the same lift enhancement when compared to the jets generated by the steady blowing mode. In the present study a ZNMF jet is adopted to apply the control.

ZNMF jets are a special case of oscillatory jets as they have zero net mass injection into the domain over one complete cycle, but importantly a non-zero momentum flow into the domain. They are typically formed by an oscillating membrane within a cavity flush-mounted below the aerodynamic surface. The cavity locally inhales and exhales the working fluid, generating a separated shear layer from its orifice [7]. ZNMF jets have successfully been applied to a range of airfoil and turbine flow configurations for separation control. Studies with application to low-pressure turbines have again illustrated improved efficiency of unsteady over steady suction, and jets normal to the wall were more effective than tangential blowing [19] [12]. The airfoil application of [17] at $Re_c = 3 \times 10^5$ found that jets closer to the uncontrolled separation point require a lower jet velocity to achieve the same lift enhancement.

Paying attention to these previous findings, [22] later undertook experiments on a NACA 0015 airfoil at $Re_c = 3 \times 10^5$, with the ZNMF jet normal to the surface and at the leading edge, which was near the uncontrolled separation point for angles of attack past the post-stall region. An LES of this flow configuration was then undertaken in [5]. This paper will provide a brief overview of both the experimental and numerical studies and then present the stability analysis of the mean velocity field from the LES.

Overview of Experimental Measurements

The parameter space explored in the experimental study of [22] is presented below non-dimensionalised on the basis of cord length (c) and freestream velocity (U_∞). The pertinent non-dimensional parameters are the Reynolds number (Re_c), forcing frequency (F^+), momentum blowing coefficient (c_μ), and for completeness an alternate measure of the jet velocity, the velocity ratio (VR). Table 1 outlines the parameter definitions, the range explored with force measurements, and the parameter set that maximised the lift enhacement. Flow visualisations were then undertaken at $\alpha = 18^\circ$ for the uncontrolled and controlled flow with the parameters maximising lift enhancment. Dye streak visualisations gave a qualitative indication of the mean velocity fields, illustrating that the control significantly reduced the mean separated region (see Fig.1). Particle Image Velocimetry (PIV) measurements were also undertaken to quantify the velocity fields.

It is assumed that the maximum lift enhancement coincides with the greatest level of reattachment and hence the most effective transition to turbulence of the laminar flow region. This assumption allows the comparison of the frequency determined in the experiments to maximise lift enhancement ($F^+_{max-lift}$) to the forcing frequency determined in the stability analysis to maximise spatial growth of a disturbance (F^+_{max-sg}).

Overview of Numerical Simulation

The study of [5] utilised the incompressible version of the code

Parameter Definition	Range Explored	Lift Enhacement Maximised with
$Re_c \equiv \frac{U_\infty c}{\nu}$	3×10^4	3×10^4
$F^+ \equiv \frac{fc}{u_\infty}$	$0.3 \leq F^+ \leq 2$	1.3
$c_\mu \equiv 2\frac{h}{c}(\frac{u_{j,rms}}{U_\infty})^2$	$0 \leq c_\mu \leq 1.38 \times 10^{-3}$	1.38×10^{-3}
$VR = \frac{u_{j,rms}}{U_\infty}$	$0 \leq VR \leq 0.7$	0.7
α	$0^\circ \leq \alpha \leq 27^\circ$	$\alpha = 18^\circ$

Table 1: Parameter exploration with force measurements in the experiments of [22]

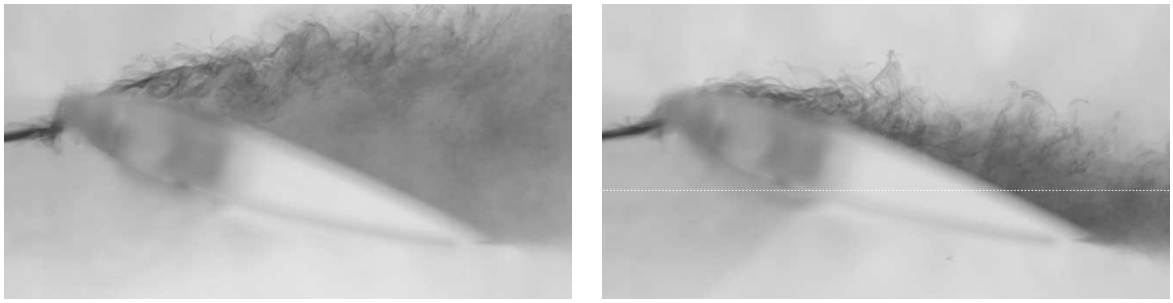

(a) (b)

Figure 1: Die streak flow visualisations of a NACA 0015 airfoil at $\alpha = 18^\circ$. (a) uncontrolled; (b) controlled. Modified from [22]

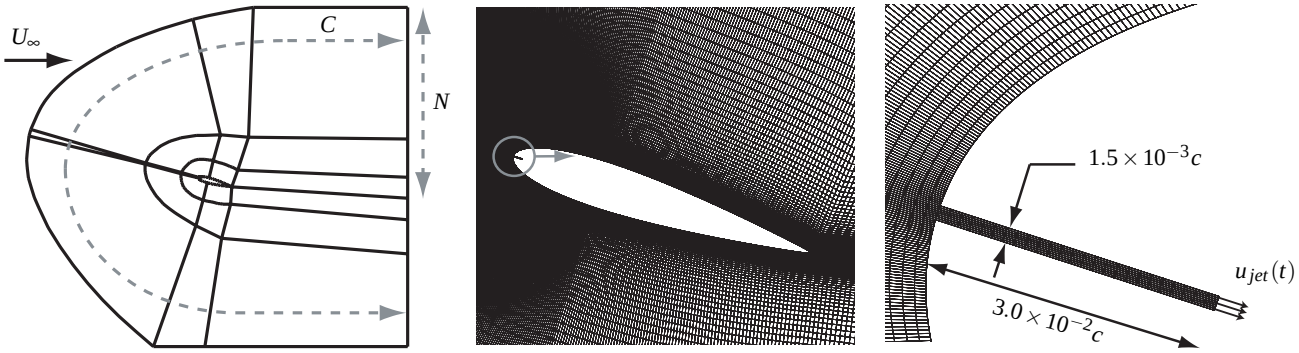

(a) (b) (c)

Figure 2: Topology of the modified C-type grid. (a) block topology; (b) body-fitted airfoil grid; (c) ZNMF jet cavity. [5]

Direction	Domain Size	Cell Count	Cell Spacing	Viscous Scaling
C	28c	808	$2 \times 10^{-4} < \Delta C/c < 1 \times 10^{-2}$	$\Delta C^+/c \leq 24$
N	6c	80	$\Delta N/c = 1.2 \times 10^{-3}$	$\Delta N^+/c \leq 3$
Z	1c	40	$\Delta Z/c = 5.0 \times 10^{-2}$	$\Delta Z^+/c \leq 150$

Table 2: LES grid spacing details of [5]

CDP to replicate the experimental study of [22]. *CDP* was developed at the *Stanford Center for Turbulence Research* and is an unstructured finite volume based solver. Numerical dissipation is minimised by discretising the continuity and momentum equations such that they discretely conserve kinetic energy. This is enforced on the pressure and convective terms using the approach outlined in [8]. The dynamic Smagorinski subgrid scale (SGS) model of [3] was adopted for the 3-D LES calculation.

A modified C-type grid of the NACA 0015 airfoil was adopted with the block topology as illustrated in Fig. 2(a). The grid was summarised by the inlet arc (C), the distance between the body and the outer boundary (N), and in the spanwise domain (Z). A Dirichlet boundary condition of $(u,v,w) = (U_\infty, 0, 0)$ was applied at the inlet, top, and bottom boundaries. A Neumann boundary condition of $\frac{\partial u}{\partial x} = 0$ was applied at the outlet and a periodic boundary condition was applied in the spanwise direction. The computational domain size, cell count, and cell spacings (non-dimensionalised by the cord and also in viscous units) are summarised in Table 2. The ZNMF jet cavity was also resolved by the grid, but note that no controlled results are presented herein. For further details on the numerical approach refer to [5].

It is acknowledged that the resolution in the spanwise direction is not adequate, and the domain size in the spanwise direction is possibly larger than necessary. The LES data presented has a $\Delta Z^+ \leq 150$, which is greater than the recommended level of $\Delta Z^+ \leq 2$ as observed in the related studies of [1] and [23]. The airfoil study of [23] also used a spanwise domain size of $0.2c$ in contrast to the domain size of $1c$ used in LES data presented. Simulations are currently being undertaken with the appropri-

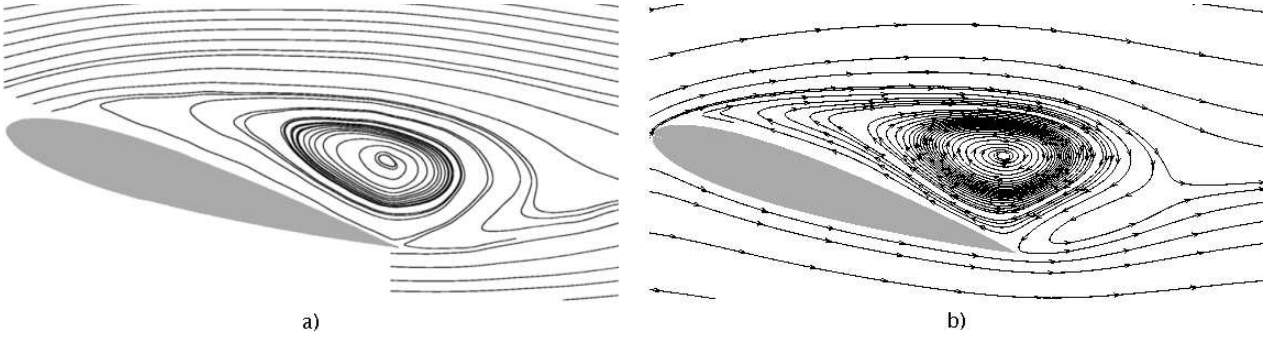

Figure 3: Mean streamlines of the natural state from: a) PIV measurement of [22]; and b) 3-D LES of [5]

ate modifications (note the cavity has also subsequently been removed). Despite the lack of resolution in the spanwise direction, the integrated forces agreed with the force measurements to within measurement error and there is a qualitative agreement with the PIV measurements as illustrated in Fig. 3. From this perspective the author assumes that the data is adequate to perform an initial stability analysis.

Stability Analysis Formulation

The stability of a fluidic system is governed by the perturbation form of the NSE to determine the effect that small perturbations have on the transition to turbulence. The perturbation form of the NSE, considering the vortical instabilities are formed by substituting the Reynold's decomposition of velocity ($u_i = \bar{u_i} + \tilde{u}_i$) and pressure ($p = \bar{p} + \tilde{p}$) into the NSE and expanding the terms. The *overbar* modifier designates the time averaged mean and the *tilde* a small fluctuating component. Assuming the mean component is not time varying, then the NSE of only the mean terms are then subtracted away to return the following system of equations

$$\frac{\partial \tilde{u}_i}{\partial x_i} = 0, \text{ and} \tag{1}$$

$$\frac{\partial \tilde{u}_i}{\partial t} + \bar{u_j}\frac{\partial \tilde{u}_i}{\partial x_j} + \tilde{u}_j\frac{\partial \bar{u_i}}{\partial x_j} + \frac{\partial \tilde{p}}{\partial x_j} - \frac{1}{Re}\frac{\partial^2 \tilde{u}_i}{\partial x_j^2} = -\tilde{u}_j\frac{\partial \tilde{u}_i}{\partial x_j}. \tag{2}$$

where $\tilde{u}_j\frac{\partial \tilde{u}_i}{\partial x_j}$ are quasi-linear terms and neglected in linear analysis methods [15].

For the present application, in the above system of equations $x_1 \equiv x$ is the wall tangential direction, $x_2 \equiv y$ is the wall normal and $x_3 \equiv z$ the spanwise. Usually for an attached semi-bounded domain a boundary layer length scale is used to non-dimensionalise the system. In this case, however, the velocity profiles of interest are all separated. Consequently the system is instead non-dimensionalised on the basis of momentum thickness (Θ_{SL}) and convection velocity ($\bar{u}_{SL}$) of the shear layer. $\bar{u}_{SL} = \frac{\bar{u}_1 + \bar{u}_2}{2}$, where $\bar{u}_1$ and $\bar{u}_2$ are the maximum and minimum velocities at the ends of the shear layer respectively.

The analysis can then be classified as being either local or global depending on the dimensionality of the mean velocity field. Let us first introduce the state vector $q = (u,v,w,p)^T$. The most general case is when all mean velocity components are non-zero and each are functions of all three spatial dimensions, such that

$$\bar{q} = (\bar{u}(x,y,z), \bar{v}(x,y,z), \bar{w}(x,y,z), \bar{p}(x,y,z)). \tag{3}$$

This mean field structure only allows Fourier decomposition in the time domain such that the perturbation vector is of the form

$$\tilde{q}(x,y,z,t) = \hat{q}(x,y,z)e^{-i\Omega_{3D}t} + c.c. \tag{4}$$

where the *hat* modifier designates the associated eigenvector and *c.c* stands for complex conjugate. Substituting the perturbation vector $\tilde{q}$ and mean field structure $\bar{q}$ into the perturbation for of the NSE, results in a 3-D eigenvalue problem [21]. If the physics of the system, however, suggest that $\frac{\partial q}{\partial z} \ll \frac{\partial q}{\partial x}$ and $\frac{\partial q}{\partial z} \ll \frac{\partial q}{\partial y}$ then the mean field can be simplified to be a function of only x and y. This case is termed *BiGlobal* with an associated 2-D mean field and perturbation vector of the form

$$\bar{q} = (u(x,y), v(x,y), 0, p(x,y)). \tag{5}$$

$$\tilde{q}(x,y,z,t) = \hat{q}(x,y)e^{ik_z z - i\Omega_{2D}t} + c.c. \tag{6}$$

resulting in a two-dimensional (2-D) eigenvalue problem [21].

Local stability analysis is applicable when the physics of the system suggest that $\frac{\partial \bar{q}}{\partial x} \ll \frac{\partial \bar{q}}{\partial y}$ and $\frac{\partial \bar{q}}{\partial z} \ll \frac{\partial \bar{q}}{\partial y}$. This means that the mean velocity field is parallel and only a function of the wall normal direction y as follows

$$\bar{q} = (u(y), 0, 0, p(y)), \tag{7}$$

with associated perturbation vector

$$\tilde{q}(x,y,z,t) = \hat{q}(y)e^{ik_x x + ik_z z - i\Omega t} + c.c. \tag{8}$$

where k_x and k_z are the complex wave numbers in the x and z directions respectively and Ω is the complex temporal eigenvalue. Substituting $\tilde{q}$ into into the perturbation form of the NSE produces a second order four-equation system called the *Orr-Sommerfeld Equations* (OSE) [10] [18]. In the invicid limit, they are termed the *Rayleigh* equations [13]. The pressure perturbation is often removed by manipulating the OSE by utilising an alternate state variable is $\tilde{q} = (\tilde{v}, \tilde{\omega}_y)^T$, where $\tilde{v}$ and $\tilde{\omega}_y$ are the wall normal velocity and vorticity perturbations respectively. After some manipulation a forth order two-equation system is produced, termed the *Orr-Sommerfeld Squire Equations* (OSSE) [20]. The generalised eigenvalue problem is stated as

$$i\Omega M\tilde{q} = L\tilde{q} \tag{9}$$

$$i\Omega \begin{pmatrix} \nabla^2 & 0 \\ 0 & I \end{pmatrix} \begin{pmatrix} \tilde{v} \\ \tilde{\omega}_y \end{pmatrix} = \begin{pmatrix} L_{OS} & 0 \\ C & L_{SQ} \end{pmatrix} \begin{pmatrix} \tilde{v} \\ \tilde{\omega}_y \end{pmatrix} \tag{10}$$

with

$$L_{OS} = -ik_x\bar{u}\nabla^2 + ik_x\frac{\partial^2 \bar{u}}{\partial y^2} + \frac{1}{Re}\nabla^4 \tag{11}$$

$$C = ik_z\frac{\partial \bar{u}}{\partial y} \tag{12}$$

$$L_{SQ} = ik_x\bar{u} - \frac{1}{Re}\nabla^2 \tag{13}$$

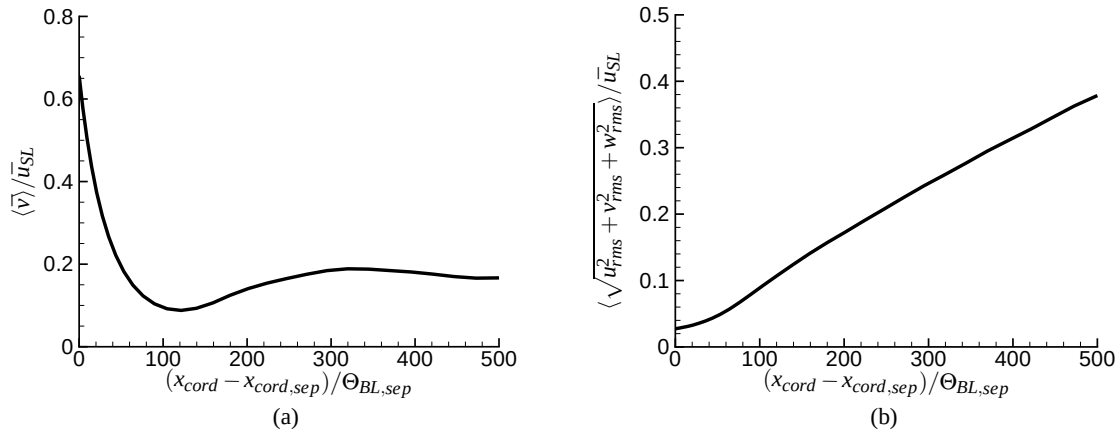

Figure 4: Indicators of valid regions for local linear stability analysis: (a) degree of parallelism quantified by $\langle\bar{v}\rangle/\bar{u}_{SL}$; (b) degree of unsteadiness quantified by $\langle\sqrt{u_{rms}^2+v_{rms}^2+w_{rms}^2}\rangle/\bar{u}_{SL}$.

where $\nabla \equiv (ik_x, \frac{\partial}{\partial y}, ik_y)$. Hence $\nabla^2 \equiv \frac{\partial^2}{\partial y^2} - k^2 I$ and $\nabla^4 \equiv \frac{\partial^4}{\partial y^4} - 2k^2 I + k^4 I$, where $k^2 \equiv k_x^2 + k_z^2$ and I is the identity matrix [15].

The above formulation captures the linear growth of a local disturbance in all three spatial dimensions and time. For an instability to be unstable, it must grow in both space and time. The imaginary components (subscript i) of the wave numbers and eigenvalues indicate the growth rates and real components (subscript r) the period of oscilation. From equation 8 it can be seen that if $k_{x,i} < 0$, $\tilde{q}$ will grow and the system is spatially unstable, and the system is temporally unstable, if $\Omega_i > 0$. Within the framework of the linearised OSSE, the most unstable eigenvalue will always have $k_z = 0$ [2]. This uncouples the equations and it is valid to solve for only the wall normal velocity perturbation $\tilde{v}$. If, however, a given system is found to be stable for all possible wave numbers it is possible that there is a period of significant initial transient growth due to non-orthogonality of the eigenvectors, even though all disturbance will decay in the limit of large t. If this is the case then it is possible to find a larger transient growth for non-zero k_z and it is important to search this space and also to solve for both $\tilde{v}$ and $\tilde{\omega}_y$ [15]. If the transient growth is large enough then non-linear effects will become important. This then provides an alternate means of the system to possibly become unstable in the limit of large t.

The present study will focus on the search of primary instabilities so the analysis will be confined to $k_z = 0$ and the solution of only $\tilde{v}$. Strictly speaking the physics of the system suggest that the *BiGlobal* formulation is the simplest model allowable for the stability analysis. The local formulation, however, will be applied to regions in flow field that best satisfy the prescribed assumptions.

Regions of Validity for Local Linear Stability Analysis

Three key assumption have been made up to this point regarding the stability analysis: one, the flow is parallel; two, the mean velocity field is steady; and three, non-linear effects are negligible. The degree to which each of these assumptions are met is discussed in this section. The most appropriate region to undertake the stability analysis is then determined as the profile that best satisfies these assumptions.

To quantify how parallel the flow actually is, $\bar{v}$ is spatially averaged (denoted by $\langle\bar{v}\rangle$) for a series of profiles normal to the airfoil surface. Figure. 4(a) illustrates this quantity plotted against the distance along the cord length (x_{cord}) from the point of separation $x_{cord,sep}$ and non-dimensionalised by the boundary layer momentum thickness at the point of separation ($\Theta_{BL,sep}$). All spatial averages were undertaken over a profile length of $500\Theta_{BL,sep}$. At the point of separation ($x_{cord} = 3.6\Theta_{BL,sep}$) $\langle\bar{v}\rangle$ is as large as $0.7\bar{u}_{SL}$ and then reaches a minimum of $0.1\bar{u}_{SL}$ at $x_{cord} = 100\Theta_{BL,sep}$. This is equivalent to a distance from the leading edge of $x_{cord} = 0.08c$. Past this point $\langle\bar{v}\rangle$ again increases and plateaus to $0.1U_\infty$ at $x_{cord} = 300\Theta_{BL,sep}$ ($0.24c$).

The second assumption is addressed by spatially averaging the magnitude of all root mean square (*rms*) velocity components. Figure. 4(b) illustrates that there is always an unsteady component from the point of separation onward. It increases from an initially modest level of $0.04\bar{u}_{SL}$ to approximately $0.4\bar{u}_{SL}$ at $x_{cord} = 500\Theta_{BL,sep}$ ($0.4c$).

The third assumption of linearity is quantified by determining the manner in which Θ_{SL} grows with position along the shear layer. In contrast to the previous two figures, where the velocity profiles were taken normal to the airfoil surface, in this case they are taken normal to the centre of the shear layer as illustrated in Fig. 5(a), and referenced with respect to the distance along the shear layer x_{SL} again from the point of separation $x_{SL,sep}$. The centre of the shear layer was determined by fitting a spline to the region of zero time averaged spanwise vorticity ($\bar{\omega}_z$). Fig. 5(b) illustrates an initial period of non-linear growth within $100\Theta_{BL,sep}$ of the point of separation. Past this point the growth is linear, and hence validates the linearity assumption over the range illustrated.

Assuming the shear layer has a parallel hyperbolic tangent profile and the flow is invicid, the result of [9] can be used to provide an indication of the frequency that will best promote reattachment. The study of [9] showed that the most spatially amplified wave grows when excited at the non-dimensional frequency $F_{max-sg} = 0.032$. This result can then be dimensionalised via

$$f_{max-sg} = \frac{F_{max-sg}\bar{u}_{SL}}{\Theta_{SL}} = \frac{0.032\bar{u}_{SL}}{\Theta_{SL}}, \qquad (14)$$

where f_{max-sg} is the associated dimensional frequency. This relationship is applied to each velocity profile normal to the shear layer and then non-dimensionalised with respect to the cord length ($F^+_{max-sg} = \frac{f_{max-sg}c}{U_\infty}$) to relate the results back to the experimental study of [22]. Figure 5(c) illustrates that

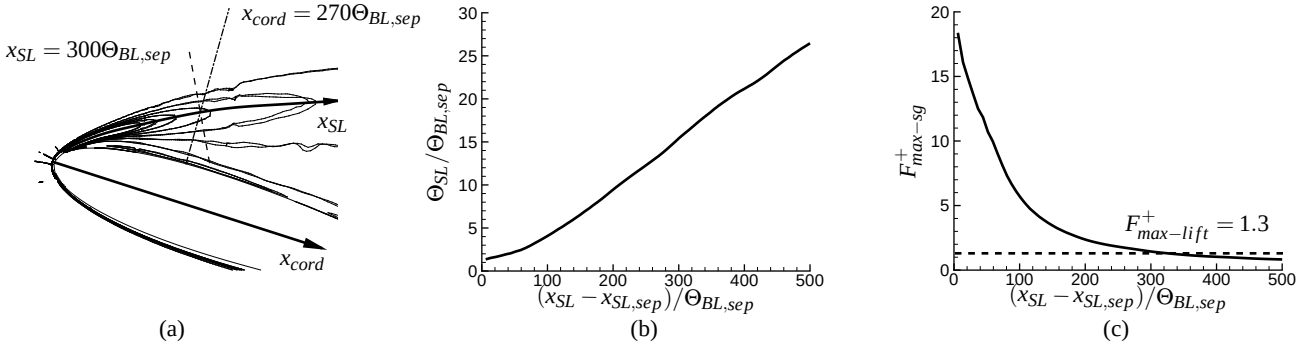

(a) (b) (c)

Figure 5: Shear layer properties: (a) location of velocity profiles, with the shear layer illustrated by contours of $\bar{\omega}_z$; (b) degree of linearity quantified by $\Theta_{SL}/\Theta_{BL,sep}$; (c) indication of best frequency to initiate transition to turbulence F^+_{max-sg}.

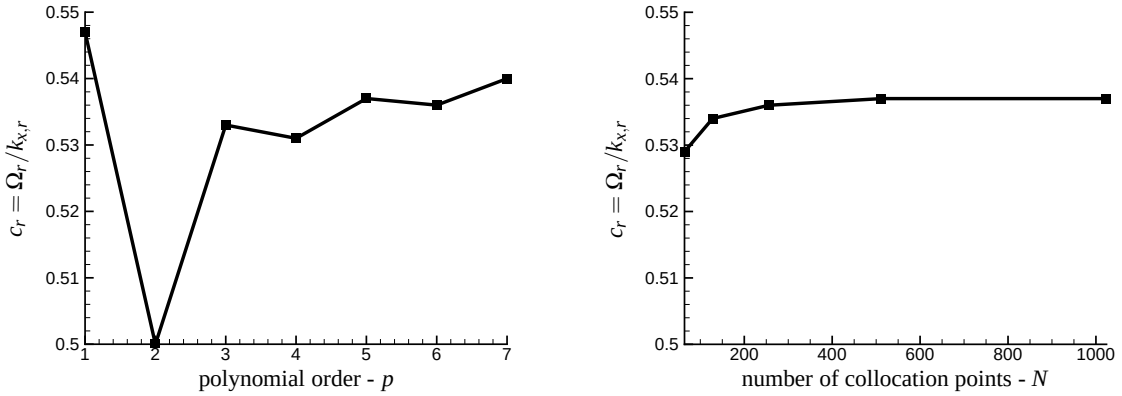

(a) (b)

Figure 6: Effect of numerical parameters on the most unstable eigenvalue of the Orr-Sommerfeld Squire equations: (a) effect of polynomial order; (b) effect of spatial resolution in wall normal direction.

F^+_{max-sg} plateaus past $x_{SL} = 300\Theta_{BL,sep}$ to a frequency similar to that determined to maximise lift in the experimental study of $F^+_{max-lift} = 1.3$. The velocity profile normal to the airfoil surface that intersects the shear layer at $x_{SL} = 300\Theta_{BL,sep}$ is $x_{cord} = 270\Theta_{BL,sep}$. The stability analysis to follow will be applied normal to the airfoil surface at this position as it is within the linear region, equally satisfies the steady and parallel flow assumption and the shear layer analysis method of [9] indicates that the frequency that would maximise the spatial growth of the disturbances is similar to that stated in the experiment.

Sensitivity of the Orr-Sommerfeld Squire Stability Analysis

The Orr-Sommerfeld Squire local stability code solves the generalised eigenvalue problem of equation 9 using a spectral Chebyshev collocation method to discretise the wall normal dimension. The *Chebyshev* derivative matrices $D^{(n)}$ replace the $\frac{\partial^n}{\partial y^n}$ operators applied to the perturbation components. For details in this approach the interested reader is referred to [11]. The code is written in *C++*, utilising the *Blitz++* library to handle the complex number mathematics and matrix operations, and *clapack* for the eigenvalue calculations.

The sensitivity of the code to the reconstruction of the mean velocity profiles and the *Chebyshev* spatial resolution is discussed in this section with application to the velocity profile at $x_{cord} = 270\Theta_{BL,sep}$. For this particular profile $\Theta_{SL} = 0.012c$, $\bar{u}_{SL} = 0.54U_\infty$ and the Reynolds number based on these parameters $Re_{\Theta_{SL}} = \frac{\bar{u}_{SL}\Theta_{SL}}{\nu} = 196$. A domain size of $80\Theta_{SL}$ is used in the following simulations.

The accuracy of the mean velocity field is very important in the analysis. Getting accurate data for $\frac{\partial^2 \bar{u}}{\partial y^2}$, required for the term L_{OS}, is the most difficult task and the source of greatest error. The error is minimised by using the unstructured discretisation within *CDP* to find all of the Cartesian second order spatial derivatives of the mean velocity field. The derivatives and the mean velocities themselves were then interpolated onto the velocity profile by fitting a 2-D polynomial surface to the LES data. The stencil of node points on the LES mesh utilised to fit the polynomial surface was selected on the basis of proximity to the point on the velocity profile required for interpolation. $\frac{\partial^2 \bar{u}}{\partial y^2}$ (where y is wall normal direction and not the Cartesian direction) was then reconstructed from the cartesian second order derivatives. The sensitivity of the most unstable eigenvalue to the polynomial order (p) was tested. Figure 6(a) illustrates an initial fluctuation in the real component of the wave speed ($c_r = \Omega_r/k_{x,r}$) and then plateaus past $p = 3$. The imaginary component ($c_i = \Omega_i/k_{x,r}$) changed negligibly in comparison. $p = 5$ was required for the velocity profiles to be completely smooth and utilised for the all of the following simulations. It is acknowledged that the largest accumulation of errors occurs at this step. The error will be quantified in the future by using an appropriate analytical test function to trace the accumulation of the error throughout the process.

The sensitivity of the spatial resolution was then tested by holding the polynomial order constant at $p = 5$ and increasing the number of Chebyshev collocation points $(N+1)$. Figure 6(b) shows a convergence of c_r at $N = 512$. This level of spatial resolution was then used for all following simulations. The scale on the y axis is the same in both Figure 6(a) and Figure 6(b) to highlight the greater variability in c_r as a result of the polynomial order. The effect of wall normal domain size was also tested and found to modify c_r a negligible amount in comparison to the polynomial order and spatial resolution.

Mapping of the Orr-Sommerfeld Squire Equations

As previously stated a system is spatially unstable if $k_{x,i} < 0$. In this section a series of unstable spatial wave numbers of varying growth rate and period are mapped to the temporal complex plane through the OSSE. For each grid point in Fig. 7(a) an eigenvalue problem is solved and the most unstable eigenvalue identified. Each grid point is then coloured by the growth rate of the eigenvalue Ω_i. The thick black line indicates the line where $\Omega_i = 0$. Fig. 7(b) is an alternate representation of the same data. Instead of being plotted on the complex spatial k_x wavenumber plane, it is plotted on the complex temporal Ω plane and now coloured with contours of spatial growth rate $k_{x,i}$. The thick black lines in each figure are equivalent. This line is important as it is the line with no temporal growth. This is representative of the ZNMF jet providing a perturbation at a constant amplitude. The task now is to identify for which temporal period Ω_r the spatial growth is a maximum. This is achieved by interpolating the values of the spatial growth rate $k_{x,i}$ onto the thick black line. The result of this interpolation is plotted in Fig. 7(c) with $k_{x,i}$ negated as a perturbation is spatially unstable for $k_{x,i} < 0$. The maximum spatial growth occurs at $\Omega_{r,max-sg} = 0.227$. The frequency that maximises spatial growth is therefore, $F_{max-sg} = \frac{\Omega_{r,max-sg}}{2\pi} = 0.036$. This is in close agreement with the previously stated result of [9] of $F_{max-sg} = 0.032$. The F_{max-sg} determined from the current analysis is dimensionalised via

$$f_{max-sg} = \frac{F_{max-sg} u_{SL}}{\Theta_{SL}} = \frac{0.036 \times 0.544 U_\infty}{0.012c} = \frac{1.64 u_\infty}{c} \quad (15)$$

and finally scaled with respect to the airfoil length scales to yield

$$F^+_{max-sg} = \frac{f_{max-sg} c}{U_\infty} = 1.64. \quad (16)$$

This is again in close agree with the frequency determined in the experimental study of [22] to maximise the lift enhancement of the airfoil of $F^+_{max-lift} = 1.3$.

The complex k_x associated with the eigenvalue with $\Omega = \Omega_{r,max-sg} + 0i$ was interpolated from the results of the eigenvalue simulations to be $k_x = 0.232 - 0.125i$. This particular wave number was simulated and produces a temporal eigenvalue of $\Omega = 0.227 + 0.002i$. This eigenvalue has no temporal growth, to two decimal places, and is assumed to be an adequate representation of the desired disturbance. The magnitude of the normalised wall normal velocity eigenvector ($|\hat{v}|$) associated with this eigenvalue is illustrated in Fig. 7(d). It is plotted along side $\bar{u}/\bar{u}_{SL}$, to illustrated that the majority of the energy within $\hat{v}$ is concentrated in the shear layer region. It is therefore evident that the excitation of the shear layer is responsible for the transition to turbulence. This causes an increase in mixing with the freestream at this station and higher momentum fluid is draw to the wall, thus promoting reattachment.

This instability can also be classed as convective. The pinch point in Fig. 7(b), designnated by the point P, indicates the location where the group velocity $c_{gr} = 0$ [6]. c_{gr} is the speed at which a wave is convected in space. If an instability is unstable where $c_{gr} = 0$, then the instability is classed as absolute, as eventually the instability will grow and fill the entire domain and remain even after the source of the instability has been removed [4]. In this case, however, the pinch point is spatially unstable (by virtue of only simulating spatially unstable wavenumbers), but temporally stable as $\Omega_i < 0$ at this point. The instability is, therefore, convective. This means that when the source of the control is removed, the the instability will convect away, and the system will return back to the initial uncontrolled state [4]. This behaviour was also observed in the experiments of [22].

Concluding Remarks

The present paper has discussed the process of undertaking a local stability analysis on an instance of laminar separation. The key issue throughout the process has been one of spatial resolution. This line of research was initiated with the experiments of [22], with PIV measurements providing an initial mean velocity field. The spatial resolution of this mean velocity field was then increased in the numerical study of [5] using the PIV measurements to validate the LES. The spatial resolution requirements for the stability analysis presented herein, however, is still greater than available from the LES. A 2-D polynomial surface was fit to the LES data to interpolate the data required for the additional spatial resolution. It is this final step that requires additional development and verification.

Despite the issues surrounding the interpolation of the mean velocity field, and the analysis not strictly adhering to the local stability assumptions, the analysis presented herein has provided an understanding of the physics of the system. The frequency determined to maximise spatial growth of a perturbation scaled with respect to the cord length $F^+_{max-sg} = 1.64$, was found to be very similar to the frequency determined in the experiments of [22] to maximise lift enhancment of $F^+_{max-lift} = 1.3$. The analysis has also highlighted that the associated instability is convective in nature and that the excitation of shear layer is the key physical mechanism for transition to turbulence.

Acknowledgements

The authors would like to acknowledge the financial contributions of the home universities. The assistance from the *Stanford Center for Turbulence Research* and the use of the code *CDP* has also been invaluable. The authors would like to thank the Victorian Partnership for Advanced Computing (VPAC) and the Australian Partnership for Advanced Computing (APAC) for the supply of the high-performance computing resources.

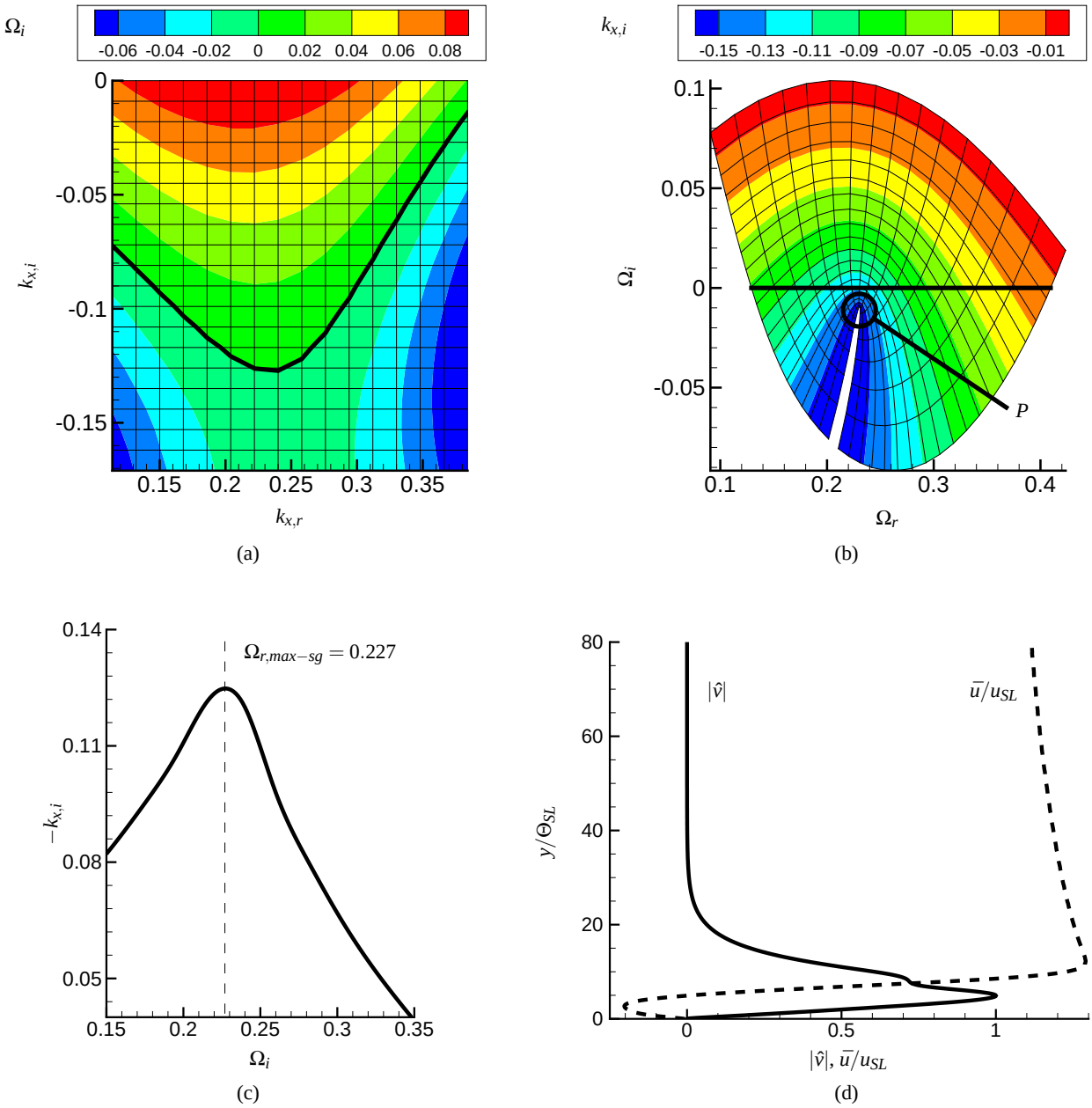

Figure 7: Mapping of Orr-Sommerfeld Squire equations for the velocity profile at $x_{cord} = 270\Theta_{BL,sep}$: (a) contours of Ω_i plotted on the complex k_x plane with the line $\Omega_i = 0$; (b) contours of $k_{x,i}$ on the complex Ω plane with the line $\Omega_i = 0$; (c) determining frequency of maximum spatial growth; (d) $\bar{u}/\bar{u}_{SL}$ (- - - -) and the eigenvector $|\hat{v}|$ (——) associated with the most temporally unstable eigenvalue $\Omega = 0.227 + 0.002i$ of the most spatially unstable wavenumber $k_x = 0.232 - 0.125i$.

References

[1] Alam, M. and Sandham, N. D., Direct numerical simulation of 'short' laminar separation bubbles with turbulent reattachment, *Journal of Fluid Mechanics*, **410**, 2000, 1–28.

[2] Drazin, P. G. and Reid, W. H., *Hydrodynamic stability*, Cambridge [Cambridgeshire] ; New York : Cambridge University Press, 1981.

[3] Germano, M., Piomelli, U., Moin, P. and Cabot, W. H., A dynamic subgrid-scale eddy viscosity model, *Phys. Fluids A*, **3**, 1991, 1760–1765.

[4] Huerre, P. and Monkewitz, P. A., Absolute and convective instabilities in free shear layers, *J. Fluid Mech.*, **159**, 1985, 151–168.

[5] Kitsios, V., Kotapati, R. B., Mittal, R., Ooi, A., Soria, J. and You, D., Numerical study and modelling of znmf jet lift enhancement of a naca0015 airfoil, in *Proceedings of the Center for Turbulence Research Summer Program, Stanford University/NASA*, 2006, 457–468, 457–468.

[6] Kupfer, K., Bers, A. and Ram, A. K., The cusp map in the complex-frequency plane for absolute instabilities, *Physics of Fluids*, **30**, 1987, 3075–3082.

[7] Lee, C., Hong, G., Ha, Q. P. and Mallinson, S. G., A piezoelectrically actuated micro synthetic jet for active flow control, *Sensors and Actuators*, **108**, 2003, pp 168–174.

[8] Mahesh, K., Constantinescu, G. and Moin, P., A numerical method for large eddy simulations in complex geometries, *J. Comput. Phys.*, **197**, 2004, 215–240.

[9] Monkewitz, P. A. and Huerre, P., Influence of the velocity ratio on the spatial instability of mixing layers, *Phys. Fluids*, **25**, 1982, 1137–1143.

[10] Orr, W. M. F., The stability or instability of the steady motions of a perfect liquid and of a viscous liquid. part i: A perfect liquid; part ii: A viscous liquid, *Proc. R. Ir. Acad. A*, **27**, 1907, 9–68 and 69–138.

[11] Peyret, R., *Spectral methods for incompressible viscous flow*, Springer, 2001.

[12] Postl, D., Gross, A. and Faselz, H., Numerical investigation of low-pressure turbine blade separation control., *AIAA-2003-614*.

[13] Rayleigh, L., On the stability, or instability, of certain fluid motions, *Proc. Lond. Math. Soc.*, **11**, 1880, 57–70.

[14] Schlichting, H. and Gersten, K., *Boundary layer theory*, Springer, Berlin, 2000, 8 edition.

[15] Schmid, P. J. and Henningson, D. S., *Stability and transition in shear flows*, Springer-Verlag, New York, 2001.

[16] Seifert, A., Bachar, T., Shepshelovich, M. and Wygnanski, I., Oscillatory blowing: A tool to delay boundary layer separation, *AIAA Journal*, **31**, 1993, pp. 2052–2060.

[17] Smith, B. and Glezer, A., The formation and evolution of synthetic jets, *Physics of Fluids*, **10**, 1998, 2281–2297.

[18] Sommerfeld, A., Ein beitrag zur hydrodynamischen erklarung der turbulenten flussigkeitsbewegungen, *Atti del IV. Congresso Internazionale dei Matematici*, **3**, 1908, 116–124.

[19] Sondergaard, R., Rivir, R. and Bons, J., Control of low-pressure turbine separation using vortex-generator jets., *Journal of propulsion and power*, **18**, 2002, 889–895.

[20] Squire, H. B., On the stability of three-dimensional disturbances of viscous fluid flow between parallel walls, *Proc. Roy. Soc. Lond. Ser. A*, **142**, 1933, 621–628.

[21] Theofilis, V., Advances in global linear instability analysis of nonparallel and three dimensional flows, *Progress in Aerospace Sciences*, **39**, 2003, 249–315.

[22] Tuck, A. and Soria, J., Active flow control over a naca 0015 airfoil using a znmf jet, in *In Proceedings of the Fifteenth Australasian Fluid Mechanics Conference (CDROM)*, The University of Sydney, 2004, paper AFMC00178.

[23] You, D. and Moin, P., Large-eddy simulation of flow separation over an airfoil with synthetic jet control, *Center for Turbulence Research Annual Research Brief*, 337–346.